Systematic analysis of protein stability associated with species-specific developmental tempo

Mitsuhiro Matsuda[1,2#], Henrik M. Hammarén[4#], Jorge Lázaro[1,3], Mikhail M. Savitski[4*], Miki Ebisuya[1,2,5*]

[1]European Molecular Biology Laboratory (EMBL) Barcelona, 08003 Barcelona, Spain.
[2]Cluster of Excellence Physics of Life, TU Dresden, Dresden, Germany.
[3]Collaboration for joint PhD degree between EMBL and Heidelberg University, Faculty of Biosciences, Heidelberg, Germany.
[4]European Molecular Biology Laboratory, Genome Biology Unit, 69117, Heidelberg, Germany.
[5]Max Planck Institute of Molecular Cell Biology and Genetics, Dresden, Germany.

#These authors contributed equally: M Matsuda, H Hammarén
*Lead contacts: M Savitski (mikhail.savitski@embl.de) or M Ebisuya (miki.ebisuya@tu-dresden.de)

Abstract

Human embryonic development is generally slower compared with mouse, and one of the model systems for such inter-species differences in developmental tempo is the segmentation clock. The oscillation period of the human segmentation clock, as measured in induced presomitic mesoderm (iPSM) cells, is two times longer than that of mouse. While the core clock gene HES7 is known to show slower protein degradation in human iPSM compared with mouse iPSM, it remains unclear whether the concept of species-specific protein stability is generalizable to other genes. Here we systematically compared the protein degradation rates of approximately 5000 genes between human and mouse iPSM by using dynamic SILAC-based proteomics, demonstrating a pervasive trend of slower protein degradation in human cells. The inter-species difference was observed not only for proteasome-mediated but also for lysosome-mediated degradation. We further investigated the effect of metabolism on the protein stability profile. Treating mouse

iPSM cells with a glycolysis inhibitor extended the segmentation clock period, aligning the protein stability profile more closely with that of human cells, though with less effect on lysosome-mediated degradation. These results highlight the universality of slower protein degradation in human development compared with mouse, and suggest metabolism as one of the modulators.

Introduction

While the molecular mechanisms and sequential events of embryonic development are generally well conserved across mammalian species, their pace of development considerably varies[1]. For example, embryogenesis from fertilization to organogenesis (i.e., until the end of Carnegie stages) takes around 60 days for humans and around 15 days for mice[2]. The motor neuron differentiation and cortical neuron maturation also take longer in humans compared with mice while both species follow similar stages of gene expression patterns[3–5]. Such inter-species differences in developmental tempo despite the conserved order and proportions of events are referred to as developmental "allochrony"[3,6–8]. One of the most well-studied model systems for allochrony is the segmentation clock, the oscillatory gene expression during embryogenesis that regulates the timing of sequential body segment formation[9]. The oscillation period of the segmentation clock is notably species-specific[6,9–13]: around 6 h in common marmosets, 5 h in humans, 4 h in rhinoceroses, cattle, and pigs, 2-3 h in rabbits and mice, 100 min in snakes, 90 min in chickens, and 30 min in zebrafish.

The segmentation clock can be effectively recapitulated through in vitro differentiation of presomitic mesoderm (PSM) from pluripotent stem cells[14–17]. The utilization of induced presomitic mesoderm (iPSM) provides access to otherwise inaccessible mammalian species, including the human and rhinoceros, and the in vitro measurements enable quantitative comparison of the species[6,8,12,18]. The 5 h- and 2.5 h-periods of the human and mouse segmentation clocks have been reproduced in vitro by several groups despite variations in the differentiation protocols and stem cell lines[14–17]. These in vitro periods are also consistent with the pace of in vivo somitogenesis. The cell-intrinsic and robust characteristics of the species-specific periods make the in vitro segmentation clock an attractive model to study allochrony.

With the iPSM platform, mechanisms for allochrony have been explored. Several biochemical reactions of the core clock gene HES7 are found to be slower in human iPSM compared with mouse[6,18]; the slower degradation rates of HES7 protein and mRNA as well as the longer delays in the HES7 gene expression processes account for the two times longer period of the human segmentation clock. The species-specific biochemical reaction speeds are also observed in the segmentation clocks of other species as well as in the differentiation processes of human and mouse motor neurons[3,12,13,19]. Nevertheless, those measurements were conducted on selected marker genes and reporters. Thus, it is unclear whether the slower protein degradation in human cells compared with mouse is specific to a particular class of genes, such as HES7, or if it is applicable across a broader spectrum of genes. Systematic comparison of protein degradation rates between human and mouse iPSM should provide insights into the mechanisms governing species-specific degradation rates.

As another mechanism for allochrony, species-specific metabolic rates have been proposed. Human iPSM cells show a lower mass-specific mitochondrial respiration rate and glycolysis rate than mouse iPSM[18]. Modulation of the electron transport chain activity and the cytosolic NAD+/NADH ratio in iPSM alters the segmentation clock periods[12,18]. Modulation of glycolytic activity perturbs PSM differentiation and somitogenesis in embryos[20–24]. Outside PSM cells, human cortical neurons have lower mitochondrial metabolic activity than mouse neurons, and stimulation of mitochondrial metabolism in human neurons accelerates their maturation[4]. However, the relationship between species-specific metabolic rates and protein degradation rates remains unclear.

In this study, we systematically measured the protein degradation rates in human iPSM, mouse iPSM, and mouse iPSM treated with a glycolysis inhibitor by using quantitative proteomics as well as independent real-time degradation assays. The obtained results revealed a pervasive trend of slower degradation rates in human cells compared with mouse and also suggested the role of metabolism as a broad modulator of protein degradation.

Results

SILAC-proteomics comparison of human and mouse iPSM cells

We performed dynamic SILAC (stable isotope labeling of amino acids in cell culture) and quantitative mass spectrometry to estimate protein degradation rates[25,26]. Human and mouse iPSM cells were derived through in vitro differentiation of human induced pluripotent stem cells (iPSCs) and mouse epiblast stem cells (EpiSCs), respectively (Fig. 1a)[6,12,16]. For both species, we employed HES7-knockout stem cell lines to suppress the segmentation clocks and prevent protein levels from oscillating during sampling. For the labeling of newly synthesized proteins, the iPSM cells were treated with SILAC medium containing heavy arginine and lysine and collected at multiple time points between 30 min to 12 h (Fig. 1a; Supplementary Fig. 1a). LC-MS/MS (liquid chromatography-coupled tandem mass spectrometry) analysis and protein copy number estimation[27] suggested that protein copy numbers per cell were similar between human and mouse iPSM cells (Supplementary Fig. 1b,c).

We determined the ratio of newly synthesized (i.e., labeled with heavy amino acids) proteins and preexisting (i.e., light) proteins and calculated the protein degradation rates as previously described[25,26] (Supplementary Fig. 2, and see also Methods). Note that the degradation rates were corrected by the protein dilution rate resulting from cell division[25]. The cell cycle time was estimated by assuming that the top 1% slowest turning-over proteins decay exclusively through dilution, not degradation. The estimated cell cycle time in human iPSM was longer than that in mouse iPSM (Supplementary Fig. 3a), indicating that protein dilution was also slower in human cells as previously reported[18]. For ease of interpretation, the cell cycle-corrected degradation rates were transformed to half-lives, which will be used throughout the rest of the study. To ensure robust estimation of half-lives, human and mouse iPSM samples were measured in three independent biological replicates, and they displayed strong reproducibility (Supplementary Fig. 3b). For the final dataset, we included all gene names with quantified half-lives in at least two out of the three replicates for each species, resulting in half-lives for 4835 mouse and 4612 human gene names, with 3630 shared across species (Fig. 1b,c; Supplementary Table 1).

Protein degradation in human cells is pervasively slower than mouse

The distribution of the measured half-lives revealed a consistent pattern of slower degradation in human iPSM compared with mouse iPSM (Fig. 1c). The median half-life

was 37 h for human and 24 h for mouse (Fig. 1b). The overall 1.5-fold change between the two species was comparable with the 2-fold change between the human and mouse HES7 degradation rates previously reported[6]. To analyze individual cases of significantly different degradation rates, we used an F-statistic approach[28,29] (Supplementary Fig. 2d-f, see also Methods), finding that among the 3630 gene names, 1753 showed significantly slower degradation in human cells while only 126 showed significantly faster degradation in human cells (Fig. 1d). The inter-species difference was more pronounced for slowly turning-over proteins than for rapidly turning-over proteins, even though proteins of all half-life decile ranks showed slower degradation in human cells (Fig. 1e). The inter-species difference in half-lives was independent of the protein's expression level (Fig. 1f; Supplementary Fig. 3c). These results demonstrated that protein degradation in human iPSM was pervasively slower than that in mouse iPSM.

Proteins in all cellular components display inter-species differences

To characterize the proteins that exhibited significant differences in half-lives between species, we performed gene ontology (GO) analyses. No GO term in molecular function (MF) and biological process (BP) classes was significantly enriched, likely reflecting pervasive inter-species differences across all functional categories. Protein classification according to the cellular component (CC) GO terms also revealed the pervasive trend of slower degradation in human iPSM compared with mouse iPSM regardless of the subcellular localization of the proteins (Fig. 2a). However, CC GO terms associated with mitochondria, endoplasmic reticulum (ER), and membranes were significantly enriched in the proteins that exhibited slower degradation in human cells (Fig. 2b). Consistent with this observation, the proteins localized in the mitochondrion and ER showed significantly larger fold changes between human and mouse half-lives compared with the average change (Fig. 2a). By contrast, the proteins in the nucleolus showed a smaller fold change, even though their degradation was still slower in human cells (Fig. 2a). These results suggested that proteins irrespective of categories turned over more slowly in human cells than in mouse and that membrane proteins tended to show larger inter-species differences.

To verify the results with an independent assay, we made several luciferase-fusion reporters representing different subcellular localizations (Supplementary Fig. 4). The nuclear reporter comprised the DNA-binding domain of HES7 and luciferase. The

mitochondrial, lysosomal, Golgi, and ER reporters employed the localization domains or full-length of ATP5MC1, LAMTOR1, NOS3, and SEC61B, respectively (Supplementary Fig. 4a). We measured the degradation rates of the localization reporters by halting their transcription and monitoring the decrease in the luciferase signal. All the localization reporters except for the Golgi reporter displayed significantly slower protein degradation in human iPSM compared with mouse iPSM (Fig. 2c,d; Supplementary Fig. 4b,5), consistent with the SILAC-proteomics results.

A potential commonality of the CC categories that showed the most significant inter-species differences (i.e., membranes, ER, and mitochondria) is that the proteins in those localizations are mostly degraded through lysosomes[30,31]. Intracellular proteins are degraded through two main mechanisms: the ubiquitin-proteasome and autophagy-lysosome systems. Degradation through the ubiquitin-proteasome system has been demonstrated to have inter-species differences: the bulk proteasome activity is lower in human iPSM compared with mouse, and HES7, the control protein that displays the inter-species difference, is ubiquitinated and degraded through proteasomes[12,18,32]. By contrast, it has been unclear if protein degradation through the autophagy-lysosome system has inter-species differences. To address this question, we inhibited the autophagy and lysosomal activities with bafilomycin A1, a vacuolar-type H+-ATPase blocker[33] (Fig. 2e; Supplementary Fig. 4c). Treatment of mouse iPSM with bafilomycin halted the degradation of the mitochondrial, lysosomal, Golgi, and ER reporters, indicating that these degradations were indeed mediated through the autophagy-lysosome system. By contrast, bafilomycin treatment did not affect the degradation of the nuclear reporter, as HES7 degradation is mediated through the ubiquitin-proteasome system[32] (Fig. 2e). Consistent with this, the degradation of the nuclear reporter was inhibited by a proteasome inhibitor MG-132 treatment (Supplementary Fig. 4d). These results collectively showed that protein degradation through not only the ubiquitin-proteasome system but also the autophagy-lysosome system was pervasively slower in human cells compared with mouse.

Inhibiting glycolytic activity decelerates the segmentation clock and protein degradation

We next investigated the effect of metabolism on the protein stability profile. While both glycolytic activity and electron transport chain activity are involved in the segmentation

clock and somitogenesis[12,18,20–24], we have recently found that a glycolysis inhibitor, 2-Deoxy-D-glucose (2DG), and an electron transport chain inhibitor, sodium azide, decelerate the segmentation clock through different mechanisms: 2DG decelerates HES7 protein degradation whereas sodium azide elongates HES7 intron processing delay[34]. Given the emphasis of this study on protein degradation, we decided to focus on the glycolysis inhibitor 2DG.

Treatment of mouse iPSM with 2DG decelerated the segmentation clock in a dose-dependent manner as described previously[34] (Fig. 3a,b): the oscillation period of mouse iPSM treated with 10 mM 2DG was 191 ± 1 min (mean ± SD), which was between the untreated mouse iPSM period (147 ± 4 min) and the reported human iPSM period (322 min)[6]. We also confirmed that the 2DG treatment decreased the glycolytic activity[34] (Fig. 3c; Supplementary Fig. 6). While mitochondrial activity negligibly increased upon 2DG treatment, the total ATP amount decreased (Fig. 3c; Supplementary Fig. 6). The 2DG treatment decelerated the protein degradation of HES7 in a dose-dependent manner[34] (Fig. 3d,e): the HES7 half-life in mouse iPSM treated with 10 mM 2DG was 34 ± 3 min (mean ± SD), which was closer to the reported half-life in human iPSM (40 min)[6] rather than untreated mouse iPSM (22 ± 0.8 min). The HES7 period extension by 2DG was limited compared with the half-life extension (compare Fig. 3b with 3e), probably because 2DG does not effectively influence other important parameters contributing to the period, such as HES7 intron processing delay[34].

To examine the impact of glycolytic activity on the global protein stability profile, we performed the dynamic SILAC-proteomics with mouse iPSM treated with 10 mM 2DG (hereafter referred to as mouse_2DG). The cell cycle time of the mouse_2DG sample was closer to that of the human sample than the mouse sample (Supplementary Fig. 3a). The distribution of the measured half-lives revealed a consistent pattern of slower degradation in mouse_2DG as compared with untreated mouse (Fig. 3f; Supplementary Table 1). Among 3945 gene names, 1359 showed significantly slower degradation in mouse_2DG while only 24 showed significantly faster degradation in untreated mouse (Fig. 3g). The half-life extension by 2DG showed a very slight tendency of being greater for highly abundant proteins (Supplementary Fig. 7). Unlike the human versus mouse sample comparison (Fig. 1e), the mouse_2DG versus mouse comparison did not exhibit larger differences in slower proteins (Fig. 3h). GO terms from broad

categories, including those associated with the proteasome, nucleolus, and ribosome, were enriched in the proteins that exhibited slower degradation in mouse_2DG (Supplementary Fig. 8a). These results indicated a broad impact of glycolytic activity on protein degradation.

Glycolysis inhibition in mouse cells mimics the human protein stability profile

The protein stability profile of the mouse_2DG sample was much more similar to that of the human sample rather than mouse (Fig. 4a). The median half-life of mouse_2DG was 36 h, closer to 37 h of human than 24 h of mouse (Fig. 4b).

However, the impacts of 2DG were somewhat localization-dependent (Fig. 4c,d; Supplementary Fig. 8b). The proteins localized in the nucleus, nucleolus, and proteasome complex showed slower degradation in mouse_2DG compared with human. By contrast, the proteins in the membranes, mitochondria, peroxisome, and ER still showed slower degradation in human compared with mouse_2DG. These results suggested that the inhibition of glycolytic activity impacted proteasome-mediated degradation more effectively than lysosome-mediated degradation. Consistent with this hypothesis, the 2DG treatment decelerated the proteasome-mediated degradation of the nuclear reporter to the extent of human, while it did not significantly influence the lysosome-mediated degradation of the mitochondrial, lysosomal, Golgi, and ER reporters (Fig. 4e; Supplementary Fig. 9,10). This difference may be because the proteasome component proteins were significantly influenced by 2DG treatment (Supplementary Fig. 8a) or because 2DG can cause protective upregulation of the autophagy activity[35]. Nevertheless, the inhibition of glycolytic activity in mouse cells mostly phenocopied the human protein stability profile.

Discussion

In this study, we demonstrated slower protein degradation in human iPSM compared with mouse across broad categories of proteins. We further mimicked the globally slower human protein degradation profile by treating mouse cells with a glycolysis inhibitor.

The extent to which the slower protein degradation in human cells compared with mouse can be attributed to differential glycolytic activities, however, is still an open question. On the one hand, the mass-specific glycolysis rates are lower in human iPSM

compared with mouse[12,18]. On the other hand, the glycolysis rates do not simply correlate with the segmentation clock periods or the HES7 protein degradation rates across multiple species or even within the same species[12,24]. How the glycolysis inhibition influences protein degradation also remains unclear. Given that both the ubiquitin-proteasome and autophagy-lysosome systems are multi-step processes that require ATP, lowering the ATP production rate may decelerate the rate-limiting steps of protein degradation. It should be noted, however, that glycolysis and its inhibitor 2DG also influence cellular signaling and glycosylation pathways[22,24,36,37]. Furthermore, the inhibition of glycolytic activity less effectively affected lysosome-mediated degradation compared with proteasome-mediated degradation, implying additional factors. The exact contribution of glycolysis inhibition to the species-specific protein stability profile is a subject of future investigation.

Previous studies measured biochemical reaction parameters of individual marker genes and reporters to investigate species-specific developmental time[3,6,12,18,19]. While these targeted measurements are precise and valuable, they carry the risk of misleading the conclusion due to various exception genes that do not follow the trend of inter-species differences. In this study, our systematic measurements unveiled a comprehensive view of the protein stability profile in the same cell type of two species, enabling the classification of genes that display inter-species differences. Protein degradation through both ubiquitin-proteasome and autophagy-lysosome systems as well as protein dilution through cell division were slower in human cells compared with mouse. The pervasively slower protein turnover in human cells may contribute to the generally slower pace of human cell differentiation and development than mouse. Even outside the developmental biology field, a recent systematic proteomics study has reported a correlation between protein stability and organismal lifespan across fibroblasts of twelve mammalian species[38]. Applying the systematic comparison of biochemical reaction parameters to more diverse cell types and diverse animal species should be informative to study inter-species differences in general biological tempo[8].

Methods

Cell cultures and PSM induction

The cell culture methods were described previously[34]. Human iPSCs (201B7 line, from RIKEN BRC #HPS0063)[39] were cultured on Matrigel-coated dishes in the StemFit medium (Ajinomoto) without feeder cells. Cells were passaged with ROCK inhibitor Y-27632 (10 μM). Ethical approval for human iPSC usage was granted by Department de Salut de la Generalitat de Catalunya (Carlos III Program). Our human PSM induction protocols have two variations: 1-step and 2-step protocols. For the 1-step protocol, 2×10^4 human iPSCs were seeded on a 35 mm dish coated with Matrigel and cultured for three days. Then the medium was changed into CDMi[40] containing SB431542 (10 μM), CHIR99021 (10 μM), DMH1 (2 μM), and bFGF (20 ng/ml); this medium is hereafter referred to as the SCDF medium. The cells were cultured in the SCDF medium for three more days. For the 2-step protocol, 2×10^4 human iPSCs were seeded on a Matrigel-coated 35 mm dish and cultured for three to four days. Then the medium was changed into CDMi containing bFGF (20 ng/ml), CHIR99021 (10 μM), and Activin A (20 ng/ml), and the cells were cultured for one day. The cells were further cultured in the SCDF medium for one more day.

Mouse EpiSCs (from RIKEN BRC #AES0204)[41] were maintained on fibronectin-coated dishes with the DMEM-F12 maintenance medium containing 15% Knockout Serum Replacement, Glutamax (2 mM), non-essential amino acids (0.1 mM), β-mercaptoethanol (0.1 mM), Activin A (20 ng/ml), bFGF (10 ng/ml), and IWR-1-endo (2.5 μM). Cells were passaged with ROCK inhibitor Y-27632 (10 μM). The medium was changed every day. For mouse PSM induction, 5×10^4 mouse EpiSCs were seeded on a Matrigel-coated 35 mm dish and cultured in the maintenance medium without IWR-1 for one day. Then the cells were cultured in the SCDF medium for 30 h.

DNA constructs and reporter cell lines

The localization reporter constructs for degradation assays (Fig. 2,4) are illustrated in Supplementary Fig. 4a. For the Hes7 oscillation assay (Fig. 3a), the mHes7 promoter-Firefly luciferase (Fluc)-NLS-PEST-stop-mHes7(w/o intron) construct[6] was used. For the Hes7 protein degradation assay (Fig. 3d), the reverse TetOne (rTetOne) promoter-mHes7 (w/o intron)-Nano luciferase (Nluc) construct[6] was used. All promoters or genes were

subcloned into the pDONR vector to create entry clones. These entry clones were recombined with the piggyBac vector[42] (a gift from K. Woltjen) by using the Multisite Gateway technology (Invitrogen). The constructs were stably introduced into the human iPSCs and mouse EpiSCs by electroporation with a 4D Nucleofector (Lonza) or using lipofectamine (Invitrogen). HES7-knockout human iPSC line was previously described[6]. Hes7-knockout mouse EpiSC line was made using the CRISPR guide constructs previously used for mouse embryonic stem (ES) cells[6]. Multiple CRISPR guide constructs were transiently introduced into EpiSCs, and the deletion of the Hes7 loci was verified by PCR. The disruption of the segmentation clock oscillation was confirmed in mouse iPSM cells derived from the Hes7-knockout EpiSCs.

SILAC samples

HES7-knockout human iPSCs and Hes7-knockout mouse EpiSCs were used to suppress the oscillations of protein levels during SILAC sampling. After the PSM induction, the SCDF medium was changed into the heavy SILAC medium: the SCDF medium containing heavy lysine ($^{13}C_6{}^{15}N_2$, Silantes) and heavy arginine ($^{13}C_6{}^{15}N_4$, Silantes). For the heavy SILAC medium, the IMDM and Ham's F-12 for SILAC (Gibco #88367 and #88424) that contain very low levels of light lysine and arginine were used. After the heavy SILAC medium treatment, the iPSM cells were harvested at each time point and lysed in 50 mM HEPES-NaOH (pH 8.5), supplemented with 1% SDS, the protease inhibitor cocktail, and benzonase. Lysates were incubated at 95°C for 5 min. Details of the PSM induction conditions and collection time points are described in Supplementary Fig. 1a.

Sample preparation for mass spectrometry

Protein concentration was measured using PierceTM BCA protein assay kit (Thermo Fisher Scientific #23225), and 10 µg protein was subjected to sample preparation for MS using a modified SP3 protocol[43]. Briefly, protein samples were precipitated onto Sera-Mag SpeedBeads (GE Healthcare #45152105050250 and #65152105050250) in the presence of 50% EtOH and 2.5% formic acid (FA) for 15 min at room temperature, followed by four washes with 70% ethanol on 0.22 µm filter plates (Millipore #MSGVN22). Proteins were digested on beads with trypsin and Lys-C (5 ng/µl final

concentration each) in 90 mM HEPES (pH 8.5), 5 mM chloroacetic acid, and 1.25 mM TCEP overnight at room temperature. Peptides were eluted by centrifugation using 2% DMSO and vacuum-dried. Dry peptides were desalted by loading them on an OASIS HLB µElution plate (Waters #186001828BA), washing twice with 0.05% FA, eluting with 80% acetonitrile (ACN), 0.05% FA, and vacuum-drying. Dried peptides were taken up in 20 mM ammonium formate (pH 10) and prefractionated into 12 fractions on an Ultimate 3000 (Dionex) HPLC using high-pH reversed-phase chromatography (running buffer A: 20 mM ammonium formate pH 10; elution buffer B: ACN) on an X-bridge column (2.1 × 10 mm, C18, 3.5 µm, Waters). Prefractionated peptides were vacuum-dried.

LC-MS/MS analysis

For LC-MS/MS analysis, peptides were reconstituted in 0.1% FA and 4% ACN and analyzed by nanoLC-MS/MS as follows:

	Replicate 1 and Replicate 2	**Replicate 3 and mouse_2DG sample**
LC instrument	Ultimate 3000 RSLC (Thermo Fisher Scientific)	
MS instrument	Orbitrap Fusion Lumos (Thermo Fisher Scientific)	Q Exactive Plus (Thermo Fisher Scientific)
Trapping cartridge	Acclaim C18 PepMap 100 (5 µm, 300 µm i.d. × 5 mm, 100 A) (Thermo Fisher Scientific)	
Analytical column	nanoEase M/Z HSS C18 T3 (100A, 1.8 µm, 75 µm × 250 mm) (Waters)	
Solvents	Solvent A: aqueous 0.1% FA; Solvent B: 0.1% FA in ACN (all solvents LC-MS grade from Fisher Scientific)	
Loading onto trapping cartridge	Solvent A, 3 min, 30 µl/min	Solvent A, 4 min, 30 µl/min
Analytical LC method	Constant flow 0.3 µl/min 120 min gradient of 2-40% of solvent B in A	
LC gradient	Solvent B in A, from 8% to 25% over 99 min, followed	solvent B in A from 4% to 25% over 89 min, followed by 25-

	by 25-40% over 5 min, followed by washing	40% over 15 min, followed by washing
MS1 mode	Positive ion, profile mode on the Orbitrap	
MS1 m/z range	300-1500 m/z	350-1400 m/z
MS1 resolution	120,000	70,000
MS1	Max. fill time of 250 ms or AGC target of 50%	Max. fill time of 100 ms or AGC target of 3e6 ions
MS2	Precursor charge: 2-7	
MS2 isolation window	1.2 m/z	1.7 m/z, Top20 method
MS2 fragmentation	30% HCD collision energy	26 NCE (normalized collision energy)
MS2 readout	IonTrap	
MS2 settings	max fill time: 50 ms / 200% normalized AGC target	max fill time: 50 ms / AGC target: 1e5
Dynamic exclusion	45 s	30 s

Data analysis

Processing of raw files. Mass spectrometry raw files were processed using IsobarQuant[44] and peptide and protein identification was obtained with Mascot 2.5.1 (Matrix Science) using a reference mouse proteome (Uniprot Proteome ID: UP000000589, downloaded May 14, 2016) or human proteome (Uniprot Proteome ID: UP000005640, downloaded June 9, 2020) modified to include known common contaminants and reversed protein sequences. Mascot search parameters were: trypsin; max. 2 missed cleavages; peptide tolerance 10 ppm; MS/MS tolerance 0.02 Da; fixed modifications: Carbamidomethyl (C); variable modifications: Acetyl (Protein N-term), Oxidation (M), SILAC heavy Arg10, Lys8.

Data filtering and preprocessing. IsobarQuant output data was analyzed on a protein level in R (https://www.R-project.org) using an in-house data analysis pipeline. In brief, protein data was filtered to remove contaminants and proteins with less than 2 unique

quantified peptide matches, as well as proteins without a SILAC heavy-to-light (H/L) ratio (i.e., cases where one of the two SILAC channels was not quantified).

Protein copy number estimation. We estimated protein copy numbers per cell using the proteomic ruler method[27]. Briefly, signal sums (heavy + light channel) were calculated for each protein in each sample, then normalized using vsn normalization[45] across all samples. A histone signal was then calculated by summing all histone vsn-normalized signal sums. Copy numbers per cell were then estimated for each protein (on a gene name level) using the following equation:

$$copy\ number\ per\ cell = \frac{individual\ protein\ signal\ sum}{mean\ MW} * \frac{DNA\ mass}{Histone\ signal\ sum} * N_A$$

where N_A is Avogadro's number, 6.022E23, and the DNA mass is the estimated total signal mass of genomic DNA in each cell (6.5E-12 g for human, and 5.9E-12 g for mouse, assuming 3.099 and 2.728 megabasepairs for human and mouse respectively and mass of a base pair of 615.9 Da[27]), and mean MW is the mean molecular weight of the protein (in case of multiple MWs mapped to a single gene name).

Fitting of protein degradation rates (half-lives). Protein degradation rates (k_{deg}) were determined as previously described[25,26]. In brief, a linear fit was used to fit ln(H/L+1) over time with the y-intercept fixed to zero. Assuming exponential degradation of all proteins and doubling of the total protein amount during one cell cycle, the slope of this line is defined by $k_{deg} + t_{cc}$, where k_{deg} is the degradation rate constant, and t_{cc} is the cell cycle (i.e., doubling) time. We estimated t_{cc} from the distribution of all positive slopes of each replicate for each species, assuming that proteins with the 1% lowest slopes turn over only by dilution ($k_{deg} = 0$) and that the slope is thus defined by t_{cc}. Protein degradation rates were then calculated by correcting for the cell cycle (k_{deg} = slope - t_{cc}). To enable mapping results across species, the subsequent analysis was done on the gene name level. Protein degradation rates were mapped to gene name level by taking the median degradation rate across all protein Uniprot IDs under one gene name, and half-lives were calculated by taking half-life $T_{1/2} = \ln 2 / k_{deg}$. Gene names were mapped from human to mouse using the human and mouse homology classes from the Jackson laboratory (https://www.informatics.jax.org/downloads/reports/HOM_MouseHumanSequence.rpt, accessed June 17, 2020). For comparisons across species, only gene names with half-lives

in at least two biological replicates were considered, and half-lives were consolidated by taking the median across replicates for each species (except for the mouse_2DG sample, where only a single biological replicate was available).

Statistical comparison of individual protein turnover. To find proteins statistically significantly differing in degradation rates across samples (human v mouse or mouse v mouse_2DG), a comparative fitting approach was used as previously described[29]. Gene name-mapped (see above) H/L ratios were first corrected for t_{cc} to enable pooling all data from biological replicates as follows.

$$corrected\ ln\left(\frac{new}{old}+1\right) = raw\ ln\left(\frac{new}{old}+1\right) - \frac{ln2}{t_{cc}}t$$

Only gene names with data in at least 3 time points per sample, and a total of at least 8 data points (for human v mouse) or 6 data points (for mouse v mouse_2DG) were included. An F-statistic was calculated for fitting a linear fit to either data from both species together (H0 model) or to each separately (H1 model) (Supplementary Fig. 2e). To account for the heteroscedasticity of the data, the resulting F-statistic was calibrated as described previously[28] by estimating the "effective degrees of freedom" (d_1, d_2) from a null dataset, where the species labels were randomized (thus reducing any differences between the two species to those occurring by chance). d_1, d_2 were estimated for four separate bins of the data depending on the number of data points available for the comparison. The calibrated F-statistic distribution across both fractions was then used to calculate p-values for each peptide using the pf() function from the stats package in R and corrected for multiple testing using Benjamini-Hochberg correction using the p.adjust() function also from the stats package. Cases with adjusted p-value <= 0.001 were considered as being significantly differing in degradation rates across samples tested.

Gene set enrichment analysis. GO terms were taken from Uniprot (downloaded from Uniprot on Dec 13, 2022) using the human gene names in our dataset and mapping to the first gene name in Uniprot. All GO term classes (Cellular component, CC; Biological process, BP; and Molecular function, MF) were considered separately. Gene set enrichment analysis was done using the list of gene names ranked according to the difference in degradation rates in human v mouse (or mouse v mouse_2DG) and the fgsea() function from the fgsea package[46] with the following parameters: minimum set

size: 15, maximum set size: 500. Only pathways with an adjusted p-value of < 0.01 as given by fgsea are shown in the figures.

Protein subcellular localization. Annotation was done based on GO cellular component terms using the following subset of GO terms: GO:0005576 (extracellular region), GO:0031012 (extracellular matrix), GO:0005886 (plasma membrane), GO:0005856 (cytoskeleton), GO:0005737 (cytoplasm), GO:0005829 (cytosol), GO:0005739 (mitochondrion), GO:0005777 (peroxisome), GO:0005764 (lysosome), GO:0005783 (ER), GO:0005794 (Golgi apparatus), GO:0005634 (nucleus), GO:0031965 (nuclear membrane), GO:0005654 (nucleoplasm), GO:0005730 (nucleolus). Proteins annotated with multiple of these terms were included in all of the annotated groups. Groups were compared with a t test using the stat_compare_means() function from the ggpubr package.

Data visualization. Figures were prepared using in-house R scripts based mainly on the ggplot2 and ggpointdensity packages. All box plots consist of the median line, box: upper and lower quartiles, whiskers: 1.5 times interquartile range, and points: outliers.

Hes7 oscillation assay

As described previously[34], mouse EpiSCs stably expressing the mHes7 promoter-Fluc-NLS-PEST-UTR reporter were used. After the PSM induction, the medium was changed into the SCDF medium containing a lower dosage of CHIR99021 (1 μM) and D-luciferin to monitor the oscillations of the Hes7 promoter-luciferase reporter signal. The iPSM cells were pretreated with different concentrations of 2DG 2 h before the medium change, and kept in the medium containing 2DG during the measurement. The luminescence signal of the whole dish was measured at each time point with Kronos Dio Luminometer (Atto). The obtained traces were analyzed with pyBOAT 0.9.12[47]. A threshold of 300 min was used for Sinc-detrending and amplitude normalization of the signal. The processed signal was then analyzed using wavelets with periods ranging from 100 to 300 min. A Fourier estimate of the wavelet analysis provided a distribution of periods and their corresponding power. The period with the maximum power for each of the signals was considered.

Metabolic rate measurement

The measurements were performed with Seahorse XF analyzer (Agilent) as described previously[34]. iPSM cells were re-seeded on a fibronectin-coated Seahorse plate (Agilent) at a density of 9.1×10^5 cells/cm^2 in 100 μl of Seahorse XF DMEM (Agilent) supplemented with glucose (20 mM), pyruvate (1 mM), and glutamine (2 mM). Cells were allowed to attach at RT for 10 min and then transferred to a 37°C incubator without CO_2 for 10 min. After that time, 400 μl of Seahorse XF DMEM medium at 37°C was added carefully to each well without disturbing the attached cells for a total of 500 μl. Cells were incubated at 37°C without CO2 for 30 more min. For the real-time ATP rate assay (Agilent), oligomycin (1 μM), rotenone (0.5 μM), and antimycin A (0.5 μM) were used. The samples were treated with different concentrations of 2DG. The Wave Desktop and online app provided by the manufacturer were used for analysis.

Degradation assay

As described previously[34], the mouse EpiSCs and human iPSCs stably expressing the rTetOne promoter-mHes7 (w/o intron)-Nluc or individual localization reporters were used. PSM cells were induced in the presence of Doxycycline (Dox; 100 ng/ml). The expression of the Nluc-fusion proteins was initiated by washing out Dox and changing the medium into CDMi containing protected furimazine (Promega). After the Nluc signal was confirmed 4-5 h later, the transcription of the fusion protein was halted by Dox (100 ng/ml) addition at time 0, and the decay of Nluc signal was monitored with Kronos Dio luminometer. To estimate the protein half-life of the reporters, the slope of log2-transformed data was calculated. A RANSAC algorithm (scikit-learn) was used to find the most linear part of the decay curve. For conditions with complex degradation dynamics, the threshold of the RANSAC algorithm was lowered to allow a better fit of the overall signal.

Data availability

The mass spectrometry proteomics data have been deposited to the ProteomeXchange Consortium via the PRIDE[48] partner repository with the dataset identifier PXD051227.

Acknowledgments

We are grateful to K. Stapornwongkul, T. Rayon, and J. Briscoe for their comments. This work was supported by EMBL; the Deutsche Forschungsgemeinschaft (DFG, German Research Foundation) under Germany's Excellence Strategy - EXC 2068 - 390729961 - Cluster of Excellence Physics of Life of TU Dresden; the European Research Council (ERC) under the European Union's Horizon 2020 research and innovation program (grant agreement No. 101002564) (to M.E.); PRESTO (grant number JP20332265) from Japan Science and Technology Agency (JST) (to M.M.); the Boehringer Ingelheim Fonds (BIF) PhD fellowship (to J.L.); H.M.H. was supported by a fellowship from the EMBL Interdisciplinary Postdoctoral (EI3POD) Programme under Marie Skłodowska-Curie Actions COFUND (grant number 664726); M.M.S. is supported by the Allen Distinguished Investigator award through the Paul G. Allen Frontiers Group; M.E. is supported by the Alexander von Humboldt Foundation in the framework of the Alexander von Humboldt Professorship endowed by the Federal Ministry of Education and Research. The human iPSC and mouse EpiSC lines were provided by the RIKEN BRC through the National BioResource Project of the MEXT, Japan.

Author contributions

M.M. and M.E. designed the work and wrote the manuscript. H.M.H. and M.M.S performed and analyzed SILAC-proteomics. M.M. prepared the SILAC samples and performed the other experiments. M.M. and J.L. analyzed the non-SILAC data. All authors contributed to the manuscript and approved the final version.

Competing interests

The authors declare no competing interests.

References

1. Ebisuya, M. & Briscoe, J. What does time mean in development? *Development* **145**, dev164368 (2018).
2. Butler, H. & Juurlink, B. H. J. *An Atlas for Staging Mammalian and Chick Embryos*. (CRC Press, Boca Raton, FL, 2018).
3. Rayon, T. *et al.* Species-specific pace of development is associated with differences in protein stability. *Science* **369**, eaba7667 (2020).
4. Iwata, R. *et al.* Mitochondria metabolism sets the species-specific tempo of neuronal development. *Science* **379**, eabn4705 (2023).
5. Ciceri, G. *et al.* An epigenetic barrier sets the timing of human neuronal maturation. *Nature* **626**, 881–890 (2024).
6. Matsuda, M. *et al.* Species-specific segmentation clock periods are due to differential biochemical reaction speeds. *Science* **369**, 1450–1455 (2020).
7. Rayon, T. Cell time: How cells control developmental timetables. *Sci. Adv.* **9**, eadh1849 (2023).
8. Lázaro, J., Sochacki, J. & Ebisuya, M. The stem cell zoo for comparative studies of developmental tempo. *Curr Opin Genet Dev* (in press).
9. Hubaud, A. & Pourquié, O. Signalling dynamics in vertebrate segmentation. *Nat. Rev. Mol. Cell Biol.* **15**, 709–721 (2014).
10. Gomez, C. *et al.* Control of segment number in vertebrate embryos. *Nature* **454**, 335–339 (2008).
11. Oates, A. C., Morelli, L. G. & Ares, S. Patterning embryos with oscillations: structure, function and dynamics of the vertebrate segmentation clock. *Development* **139**, 625–639 (2012).
12. Lázaro, J. *et al.* A stem cell zoo uncovers intracellular scaling of developmental tempo across mammals. *Cell Stem Cell* **30**, 938-949.e7 (2023).
13. Conrad, J. V. *et al.* Efficient derivation of transgene-free porcine induced pluripotent stem cells enables in vitro modeling of species-specific developmental timing. *Stem Cell Rep.* **18**, 2328–2343 (2023).
14. Matsumiya, M., Tomita, T., Kobayashi, K., Isomura, A. & Kageyama, R. ES cell-derived presomitic mesoderm-like tissues for analysis of synchronized oscillations in the segmentation clock. *Development* dev.156836 (2018) doi:10.1242/dev.156836.
15. Chu, L.-F. *et al.* An In Vitro Human Segmentation Clock Model Derived from Embryonic Stem Cells. *Cell Rep.* **28**, 2247-2255.e5 (2019).
16. Matsuda, M. *et al.* Recapitulating the human segmentation clock with pluripotent stem cells. *Nature* **580**, 124–129 (2020).
17. Diaz-Cuadros, M. *et al.* In vitro characterization of the human segmentation clock. *Nature* **580**, 113–118 (2020).
18. Diaz-Cuadros, M. *et al.* Metabolic regulation of species-specific developmental rates. *Nature* **613**, 550–557 (2023).
19. Hoyle, N. P. & Ish-Horowicz, D. Transcript processing and export kinetics are rate-limiting steps in expressing vertebrate segmentation clock genes. *Proc. Natl. Acad. Sci.* **110**, (2013).
20. Oginuma, M. *et al.* A Gradient of Glycolytic Activity Coordinates FGF and Wnt Signaling during Elongation of the Body Axis in Amniote Embryos. *Dev. Cell* **40**, 342-353.e10 (2017).

21. Bulusu, V. *et al.* Spatiotemporal Analysis of a Glycolytic Activity Gradient Linked to Mouse Embryo Mesoderm Development. *Dev. Cell* **40**, 331-341.e4 (2017).
22. Oginuma, M. *et al.* Intracellular pH controls WNT downstream of glycolysis in amniote embryos. *Nature* **584**, 98–101 (2020).
23. Miyazawa, H. *et al.* Glycolytic flux-signaling controls mouse embryo mesoderm development. *eLife* **11**, e83299 (2022).
24. Miyazawa, H. *et al.* Glycolysis–Wnt signaling axis tunes developmental timing of embryo segmentation. Preprint at https://doi.org/10.1101/2024.01.22.576629 (2024).
25. Schwanhäusser, B. *et al.* Global quantification of mammalian gene expression control. *Nature* **473**, 337–342 (2011).
26. Mathieson, T. *et al.* Systematic analysis of protein turnover in primary cells. *Nat. Commun.* **9**, 689 (2018).
27. Wiśniewski, J. R., Hein, M. Y., Cox, J. & Mann, M. A "Proteomic Ruler" for Protein Copy Number and Concentration Estimation without Spike-in Standards. *Mol. Cell. Proteomics* **13**, 3497–3506 (2014).
28. Childs, D. *et al.* Nonparametric Analysis of Thermal Proteome Profiles Reveals Novel Drug-binding Proteins*. *Mol. Cell. Proteomics* **18**, 2506–2515 (2019).
29. Hammarén, H. M., Geissen, E.-M., Potel, C. M., Beck, M. & Savitski, M. M. Protein-Peptide Turnover Profiling reveals the order of PTM addition and removal during protein maturation. *Nat. Commun.* **13**, 7431 (2022).
30. Klionsky, D. J. & Emr, S. D. Autophagy as a Regulated Pathway of Cellular Degradation. *Science* **290**, 1717–1721 (2000).
31. Huber, L. A. & Teis, D. Lysosomal signaling in control of degradation pathways. *Curr. Opin. Cell Biol.* **39**, 8–14 (2016).
32. Hirata, H. *et al.* Instability of Hes7 protein is crucial for the somite segmentation clock. *Nat. Genet.* **36**, 750–754 (2004).
33. Yamamoto, A. *et al.* Bafilomycin A1 Prevents Maturation of Autophagic Vacuoles by Inhibiting Fusion between Autophagosomes and Lysosomes in Rat Hepatoma Cell Line, H-4-II-E Cells. *Cell Struct. Funct.* **23**, 33–42 (1998).
34. Matsuda, M., Lazaro, J. & Ebisuya, M. Metabolic activities are selective modulators for individual segmentation clock processes. Preprint at https://doi.org/10.1101/2024.06.04.597451 (2024).
35. Xi, H. *et al.* 2-Deoxy-d-glucose activates autophagy via endoplasmic reticulum stress rather than ATP depletion. *Cancer Chemother. Pharmacol.* **67**, 899–910 (2011).
36. Dingare, C., Cao, D., Yang, J. J., Sozen, B. & Steventon, B. Mannose controls mesoderm specification and symmetry breaking in mouse gastruloids. *Dev. Cell* S1534580724001989 (2024) doi:10.1016/j.devcel.2024.03.031.
37. Stapornwongkul, K. S. *et al.* Metabolic control of germ layer proportions through regulation of Nodal and Wnt signalling. Preprint at https://doi.org/10.1101/2023.12.04.569862 (2023).
38. Swovick, K. *et al.* Interspecies Differences in Proteome Turnover Kinetics Are Correlated With Life Spans and Energetic Demands. *Mol. Cell. Proteomics* **20**, 100041 (2021).
39. Takahashi, K. *et al.* Induction of Pluripotent Stem Cells from Adult Human Fibroblasts by Defined Factors. *Cell* **131**, 861–872 (2007).

40. Wataya, T. *et al.* Minimization of exogenous signals in ES cell culture induces rostral hypothalamic differentiation. *Proc. Natl. Acad. Sci.* **105**, 11796–11801 (2008).
41. Sugimoto, M. *et al.* A Simple and Robust Method for Establishing Homogeneous Mouse Epiblast Stem Cell Lines by Wnt Inhibition. *Stem Cell Rep.* **4**, 744–757 (2015).
42. Woltjen, K. *et al.* piggyBac transposition reprograms fibroblasts to induced pluripotent stem cells. *Nature* **458**, 766–770 (2009).
43. Hughes, C. S. *et al.* Ultrasensitive proteome analysis using paramagnetic bead technology. *Mol. Syst. Biol.* **10**, 757 (2014).
44. Franken, H. *et al.* Thermal proteome profiling for unbiased identification of direct and indirect drug targets using multiplexed quantitative mass spectrometry. *Nat. Protoc.* **10**, 1567–1593 (2015).
45. Huber, W., Von Heydebreck, A., Sültmann, H., Poustka, A. & Vingron, M. Variance stabilization applied to microarray data calibration and to the quantification of differential expression. *Bioinformatics* **18**, S96–S104 (2002).
46. Korotkevich, G. *et al.* Fast gene set enrichment analysis. Preprint at https://doi.org/10.1101/060012 (2019).
47. Mönke, G., Sorgenfrei, F. A., Schmal, C. & Granada, A. E. Optimal time frequency analysis for biological data - pyBOAT. *bioRxiv* 2020.04.29.067744 (2020) doi:10.1101/2020.04.29.067744.
48. Perez-Riverol, Y. *et al.* The PRIDE database resources in 2022: a hub for mass spectrometry-based proteomics evidences. *Nucleic Acids Res.* **50**, D543–D552 (2022).

Figure legends

Figure 1 Pervasively slow protein degradation in human iPSM compared with mouse

a, Experimental workflow of dynamic SILAC-based proteomics. Human and mouse iPSM cells were derived from human induced pluripotent stem cells (iPSCs) and mouse epiblast stem cells (EpiSCs), respectively, and treated with the heavy SILAC medium from 0.5 h to 12 h for the labeling of newly synthesized proteins. Following LC-MS/MS analysis and peptide quantification, the degradation rate of each protein was calculated based on the ratio of the heavy (new) to light (old) proteins at multiple points. The effect of protein dilution through cell division was compensated. **b,** The distribution and median of protein half-lives in mouse and human iPSM. N = 4835 (mouse), 4612 (human). **c,** Scatter plot comparing protein half-lives measured in human and mouse iPSM. N = 3630. **d,** Volcano plot showing proteins with significantly longer (blue) or shorter (orange) half-lives in human cells compared with mouse. The x axis shows the difference in fit between the two species signed by the difference in slope: $\text{sign}(\Delta\text{slope})*\sqrt{(RSS0-RSS1)}$, where RSS0 and RSS1 are the residual sums of squares of the fits for the H0 and H1 model respectively. The y axis shows the F-statistic, a statistical measure of significance, where large values denote greater significance. Proteins with significantly different half-lives (p-value adjusted for multiple testing <= 0.001) are colored. N = 3630. See Methods as well as Supplementary Fig. 2 for more details on the comparative fitting approach. **e,** Fold changes between human and mouse half-lives that were classified according to the human half-lives. **f,** Fold changes between human and mouse half-lives were evenly distributed across the median protein abundance of human and mouse. N = 3630. a.u.: arbitrary units. **b,e,** Box plots consist of median line, box: upper and lower quartiles, whiskers: 1.5 times interquartile range, and points: outliers.

Figure 2 Slower degradation in human iPSM for all protein categories

a, Fold changes between human and mouse half-lives classified according to the Gene Ontology (GO) cellular component (CC) terms. Box plots consist of median line, box: upper and lower quartiles, whiskers: 1.5 times interquartile range, and points: outliers. P-value is from a t test of each annotation group against the reference group of all proteins adjusted for multiple testing. **: $p < 0.01$, ***: $p < 0.001$. Cases with $p > 0.05$ are not

shown. Note that proteins localized in the mitochondrion and ER showed significantly larger fold changes in half-lives compared to the average fold change (normal asterisks), while proteins in the nucleolus showed a significantly smaller fold change compared to the average despite still a longer half-life in human than mouse (asterisk in parentheses). **b,** GO CC terms significantly enriched in proteins that showed longer half-lives in human iPSM compared with mouse. P-values are probability estimates that the given enrichment/depletion of the particular gene sets are non-random (see fgsea[46]) adjusted for multiple testing using the Benjamini-Hochberg correction. GO terms with adjusted p-value < 0.01 are shown. NES: Normalized Enrichment Score. **c,** Degradation assays of localization reporters in human and mouse iPSM. The transcription of the localization reporters fused with Nano luciferase (Nluc) was halted upon the addition of doxycycline (Dox) at time 0, and the decay of the luciferase activity was monitored. **d,** Protein half-lives of the localization reporters estimated from c and Supplementary Fig. 4,5. Graph indicates mean ± SD (N = 3). P-values are from t test. **e,** Degradation assays of localization reporters in the presence of a lysosomal inhibitor bafilomycin A1. Mouse iPSM was treated with bafilomycin from 4 h before Dox addition. Control (mouse) data are the same as c. **c,e,** Shading indicates mean ± SD (N = 3).

Figure 3 Effects of glycolysis inhibition on the segmentation clock and protein degradation

a, Dose-dependent effect of a glycolysis inhibitor 2-Deoxy-D-glucose (2DG) on the segmentation clock period. Mouse iPSM was pre-treated with 2DG for 2 h, and the oscillatory activity of the Hes7 promoter-luciferase reporter was monitored. The signal has been detrended and amplitude-normalized. **b,** Hes7 oscillation periods estimated from a. Human data is from Matsuda et al, Science (2020)[6]. **c,** ATP production rates measured by the Seahorse analyzer. The glycolytic ATP production rate (glycoATP), mitochondrial ATP production rate (mitoATP), and total ATP production rate were estimated from Supplementary Fig. 6. The ratio of induced rates (after adding 2DG) to basal rates (before 2DG) is shown. **d,** Dose-dependent effect of 2DG on Hes7 protein degradation. Mouse iPSM was pre-treated with 2DG from 4 h before Dox addition. The transcription of Hes7-Nluc was halted upon Dox addition at time 0, and the decay of the luciferase activity was monitored. **e,** Hes7 protein half-life calculated from d. Human data is from Matsuda et al,

Science (2020)[6]. **f,** Scatter plot comparing protein half-lives measured in mouse iPSM treated with 10 mM 2DG (mouse_2DG) and untreated mouse iPSM (mouse). N = 4083. **g,** Volcano plot showing proteins with significantly longer (blue) or shorter (magenta) half-lives in mouse_2DG compared with mouse. The x axis shows the difference in fit between the two samples signed by the difference in slope: sign(Δslope)*√(RSS0−RSS1), where RSS0 and RSS1 are the residual sums of squares of the fits for the H0 and H1 model respectively. The y axis shows the F-statistic. Proteins with significantly different half-lives (p-value adjusted for multiple testing <= 0.001) are colored. N = 3945. See Methods as well as Supplementary Fig. 2 for more details. **h,** Fold changes between mouse_2DG and mouse half-lives that were classified according to the human half-lives, similarly to Fig. 1e. Box plots consist of median line, box: upper and lower quartiles, whiskers: 1.5 times interquartile range, and points: outliers. **a,d,** Shading indicates mean ± SD (N = 3). **b,c,e,** Graph indicates mean ± SD (N = 3). P-values are from two-sided Dunnett's test against the indicated controls.

Figure 4 Similarities of protein stability profiles between mouse iPSM treated with 2DG and human iPSM

a, Scatter plot comparing protein half-lives measured in human iPSM (human) and mouse iPSM treated with 10 mM 2DG (mouse_2DG). N = 3395. **b,** The distribution and median of half-lives in mouse, human, and mouse_2DG. N = 4835 (mouse), 4612 (human), 4517 (mouse_2DG). **c,** Fold changes between human and mouse_2DG half-lives classified according to the GO CC terms. P-value is from a t test of each annotation group against the reference group of all proteins adjusted for multiple testing. *: $p < 0.05$, **: $p < 0.01$, ***: $p < 0.001$, ****: $p < 0.0001$. Cases with $p > 0.05$ are not shown. Note that proteins localized in the plasma membrane, mitochondrion, peroxisome, and ER showed significantly larger fold changes in half-lives compared to the average fold change (normal asterisks), while proteins in the nucleus, nucleoplasm, and nucleolus showed significantly smaller fold changes compared to the average (asterisks in parentheses). **d,** GO CC terms significantly enriched in genes that showed faster or slower degradation in human compared with mouse_2DG. P-values are probability estimates that the given enrichment/depletion of the particular gene sets are non-random (see fgsea[46]) adjusted for multiple testing using the Benjamini-Hochberg correction. GO terms with adjusted p-

value < 0.01 are shown. **e,** Protein half-lives of the localization reporters in the presence of 2DG estimated from supplementary Fig. 9,10. Human data are from Fig. 2d. Graph indicates mean ± SD (N = 3). P-values are from t test. **b,c,** Box plots consist of median line, box: upper and lower quartiles, whiskers: 1.5 times interquartile range, points: outliers.

Supplementary Figure 1 SILAC samples

a, Sample preparation for dynamic SILAC. The culture conditions and sample collection time points are shown. **b,** Protein copy numbers per cell in mouse and human iPSM cells as estimated using the proteomic ruler method (see Methods). N = 6715 (mouse), 6940 (human). P-value is from a t test. Box plot consists of median line, box: upper and lower quartiles, whiskers: 1.5 times interquartile range, points: outliers. **c,** Scatter plot comparing protein copy numbers per cell measured in human and mouse iPSM. N = 5345.

Supplementary Figure 2 SILAC data analysis

a, Principle of dynamic SILAC. The ratio of new (in this case peptides carrying heavy-labeled amino acids) to old (light) peptides was measured on the MS1 level on the mass spectrometer. **b**, Equations describing the change in new and old proteins assuming a steadily-growing (cell cycle time t_{cc}) but otherwise steady-state proteome. **c,** The first equation in b defines a straight line of ln(new/old + 1) over time with slope k_{deg} + ln2/t_{cc}. k_{deg}: degradation rate constant. **d**, To compare degradation rates across samples, the measured signal was first corrected for t_{cc}, yielding a straight line with slope k_{deg}. **e**, Comparative fitting approach. For each protein, it was estimated whether the data from two samples (e.g., mouse and human iPSM cells) were better fitted by two separate linear fits (H1 model), or whether a single fit was sufficient (H0 model). **f**, Using the residuals from the fits in e, an F-statistic was calculated to estimate the increase in goodness of fit when going from H0 to H1. For the estimation of the term d_2/d_1, see Methods and references therein.

Supplementary Figure 3 Cell cycle time estimation for SILAC samples

a, The cell cycle time was estimated by using the top 1% of the slowest degradation rates for each replicate. Graph indicates mean ± SD. **b,** Scatterplots comparing the replicates

of SILAC samples. **c,** Fold changes between human and mouse half-lives were evenly distributed across the median protein abundance of human and mouse. The color code is based on Fig. 1d. N = 3630.

Supplementary Figure 4 Degradation assays of localization reporters

a, Schematic representation of the localization reporter constructs. rTetOne: reverse TetOne; aa: amino acids; Nluc: Nano luciferase. The coding sequence (CDS) and 3' untranslated region (UTR) of human HES7 gene were added to destabilize the construct mRNA. **b,** Degradation assays of localization reporters in human and mouse iPSM. The transcription of the localization reporters was halted upon the addition of Dox at time 0, and the decay of the luciferase activity was monitored. **c,** Degradation assays of localization reporters in the presence of a lysosomal inhibitor bafilomycin A1. Mouse iPSM was treated with bafilomycin from 4 h before Dox addition. Control (mouse) data are the same as b. **d,** Degradation assays of the nuclear localization reporter in the presence of a proteasome inhibitor MG-132. Mouse iPSM was treated with 10 μM MG-132 together with Dox at time 0. **b-d,** Shading indicates mean ± SD (N = 3).

Supplementary Figure 5 Half-life estimation in human and mouse iPSM cells

Fitting of protein degradation shown in Fig. 2c and Supplementary Fig. 4b. Dashed lines indicate the most linear region considered by the RANSAC algorithm for the fitting. Slope of the fitted line is shown, and it was converted to the half-life using the equation: half-life = -1/slope.

Supplementary Figure 6 Metabolic rate measurements

Mouse iPSM was treated with different concentrations of 2DG and measured by the Seahorse analyzer. Graph indicates mean ± SD (N = 3). **a,** Proton efflux rate (PER). **b,** Oxygen consumption rate (OCR). Oligomycin (Oligo) and Rotenone + Antimycin A (Rot + AA) were added at the marked time points. **c,** Basal (before adding 2DG) and induced (after 2DG) ATP production rates measured from a,b.

Supplementary Figure 7 The effects of 2DG on half-lives

Fold changes between mouse_2DG and mouse half-lives across the median protein abundance of mouse_2DG and mouse. a.u.: arbitrary units. N = 3741. The color code in b is based on Fig. 3g.

Supplementary Figure 8 GO analysis

a, GO cellular component (CC), molecular function (MF), and biological process (BP) terms statistically significantly enriched in genes that showed slower degradation in mouse_2DG compared with mouse. **b,** GO BP terms statistically significantly enriched in genes that showed slower degradation in mouse_2DG compared with human. **a,b,** P-values are probability estimates that the given enrichment/depletion of the particular gene sets are non-random (see fgsea[46]) adjusted for multiple testing using the Benjamini-Hochberg correction. GO terms with adjusted p-value < 0.01 are shown.

Supplementary Figure 9 Degradation assays of localization reporters in the presence of 2DG

Degradation assays of the localization reporters in mouse iPSM treated with 2DG. The transcription of the localization reporters was halted by Dox at time 0, and 10 mM 2DG was added from 4 h before Dox addition. Shading indicates mean ± SD (N = 3).

Supplementary Figure 10 Half-life estimation in mouse iPSM treated with 2DG

Fitting of protein degradation shown in Supplementary Fig. 9. Dashed lines indicate the most linear region considered by the RANSAC algorithm for the fitting. Slope of the fitted line is shown, and it was converted to the half-life using the equation: half-life = -1/slope.

Supplementary Table 1

Measured half-lives for ~5000 proteins in mouse, human, and mouse_2DG samples.

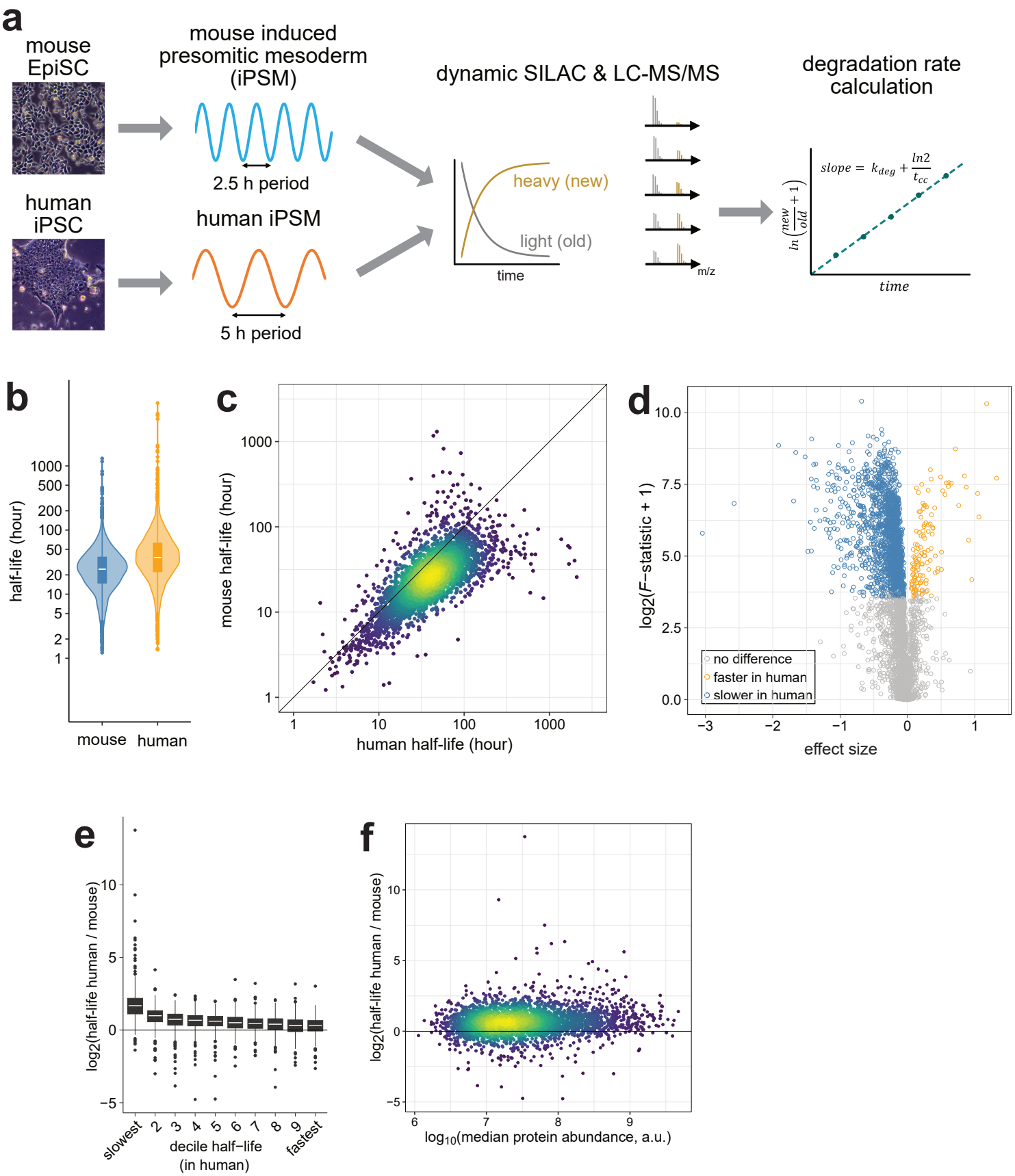
a
mouse EpiSC
mouse induced presomitic mesoderm (iPSM)
2.5 h period
human iPSC
human iPSM
5 h period
dynamic SILAC & LC-MS/MS
heavy (new)
light (old)
time
m/z
degradation rate calculation
slope = $k_{deg} + \frac{ln2}{t_{cc}}$
$ln\left(\frac{new}{old}+1\right)$
time
b
half-life (hour)
mouse
human
c
mouse half-life (hour)
human half-life (hour)
d
log2(F−statistic + 1)
effect size
no difference
faster in human
slower in human
e
log2(half-life human / mouse)
slowest
decile half−life (in human)
fastest
f
log2(half-life human / mouse)
log10(median protein abundance, a.u.)

Fig. 1

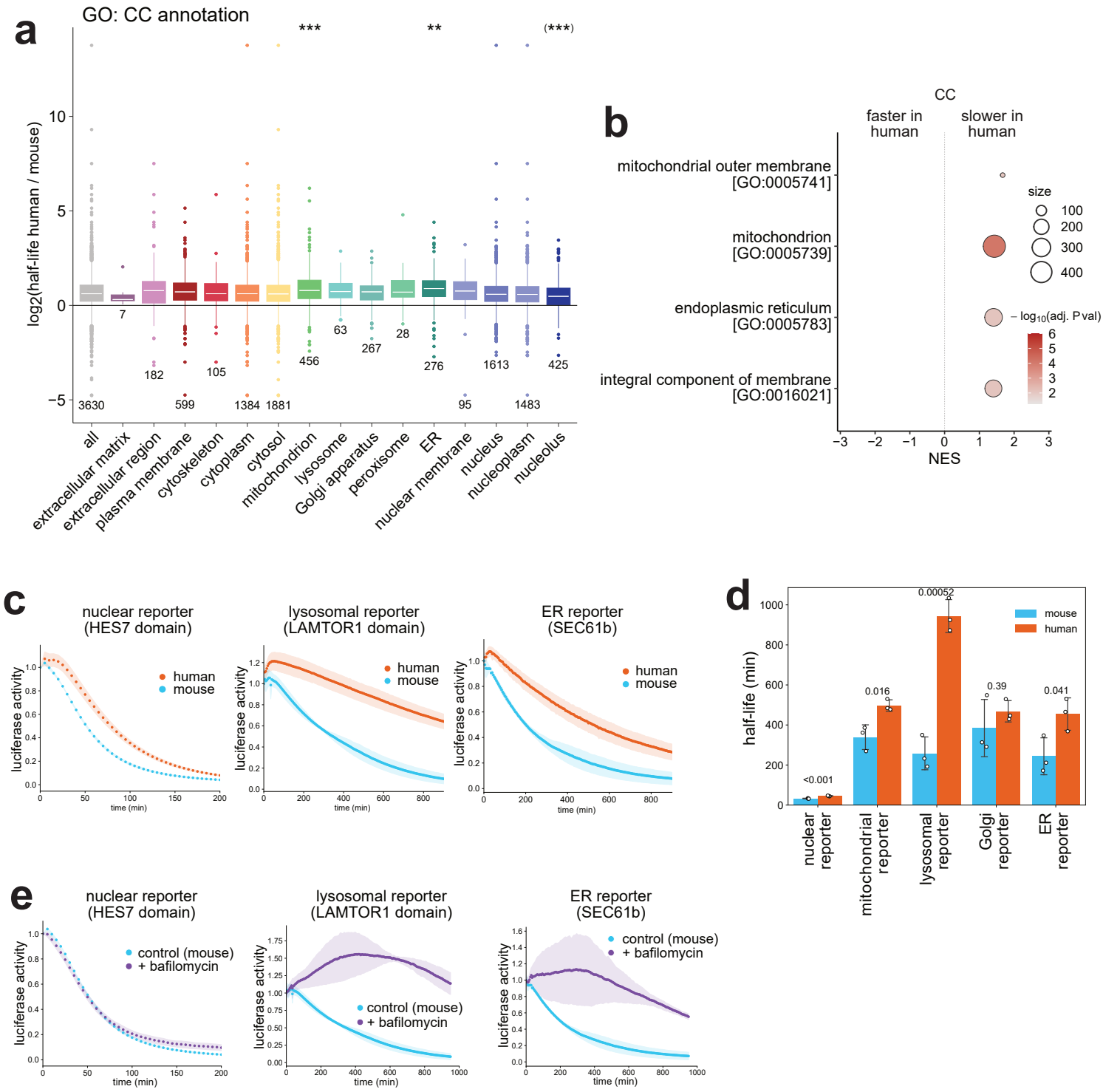
a
GO: CC annotation
log2(half-life human / mouse)
***
**
(***)
3630
7
182
599
105
1384
1881
456
63
267
28
276
95
1613
1483
425
all
extracellular matrix
extracellular region
plasma membrane
cytoskeleton
cytoplasm
cytosol
mitochondrion
lysosome
Golgi apparatus
peroxisome
ER
nuclear membrane
nucleus
nucleoplasm
nucleolus
b
CC
faster in human
slower in human
mitochondrial outer membrane [GO:0005741]
mitochondrion [GO:0005739]
endoplasmic reticulum [GO:0005783]
integral component of membrane [GO:0016021]
size
100
200
300
400
− log10(adj. P val)
NES
c
nuclear reporter (HES7 domain)
lysosomal reporter (LAMTOR1 domain)
ER reporter (SEC61b)
human
mouse
luciferase activity
time (min)
d
half-life (min)
mouse
human
<0.001
0.016
0.00052
0.39
0.041
nuclear reporter
mitochondrial reporter
lysosomal reporter
Golgi reporter
ER reporter
e
control (mouse)
+ bafilomycin

Fig. 2

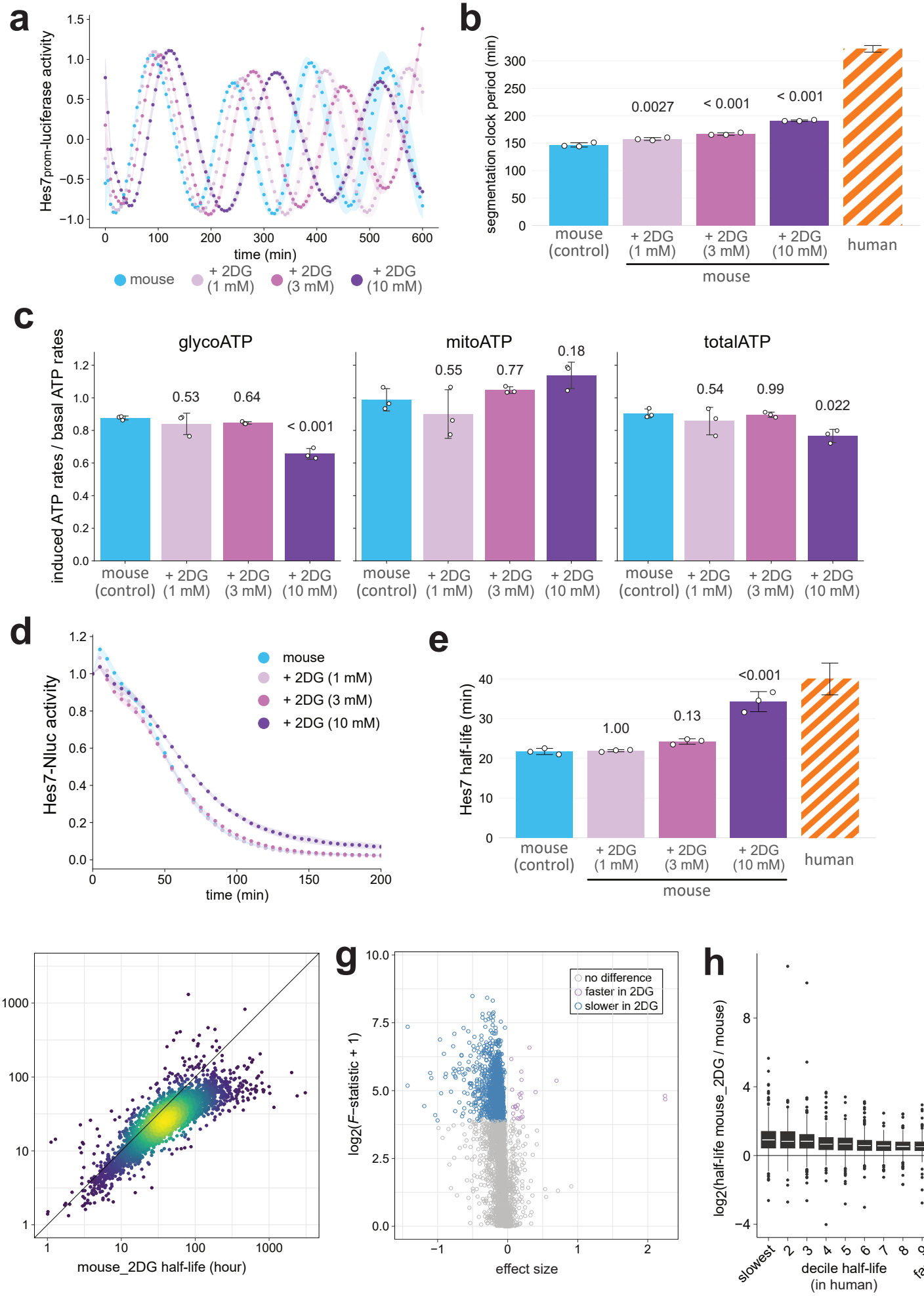
a
Hes7prom-luciferase activity
time (min)
mouse
+ 2DG (1 mM)
+ 2DG (3 mM)
+ 2DG (10 mM)
b
segmentation clock period (min)
0.0027
< 0.001
< 0.001
mouse (control)
+ 2DG (1 mM)
+ 2DG (3 mM)
+ 2DG (10 mM)
human
mouse
c
induced ATP rates / basal ATP rates
glycoATP
mitoATP
totalATP
0.53
0.64
< 0.001
0.55
0.77
0.18
0.54
0.99
0.022
d
Hes7-Nluc activity
time (min)
mouse
+ 2DG (1 mM)
+ 2DG (3 mM)
+ 2DG (10 mM)
e
Hes7 half-life (min)
1.00
0.13
<0.001
f
mouse half-life (hour)
mouse_2DG half-life (hour)
g
log2(F-statistic + 1)
effect size
no difference
faster in 2DG
slower in 2DG
h
log2(half-life mouse_2DG / mouse)
slowest
decile half-life (in human)
fastest

Fig. 3

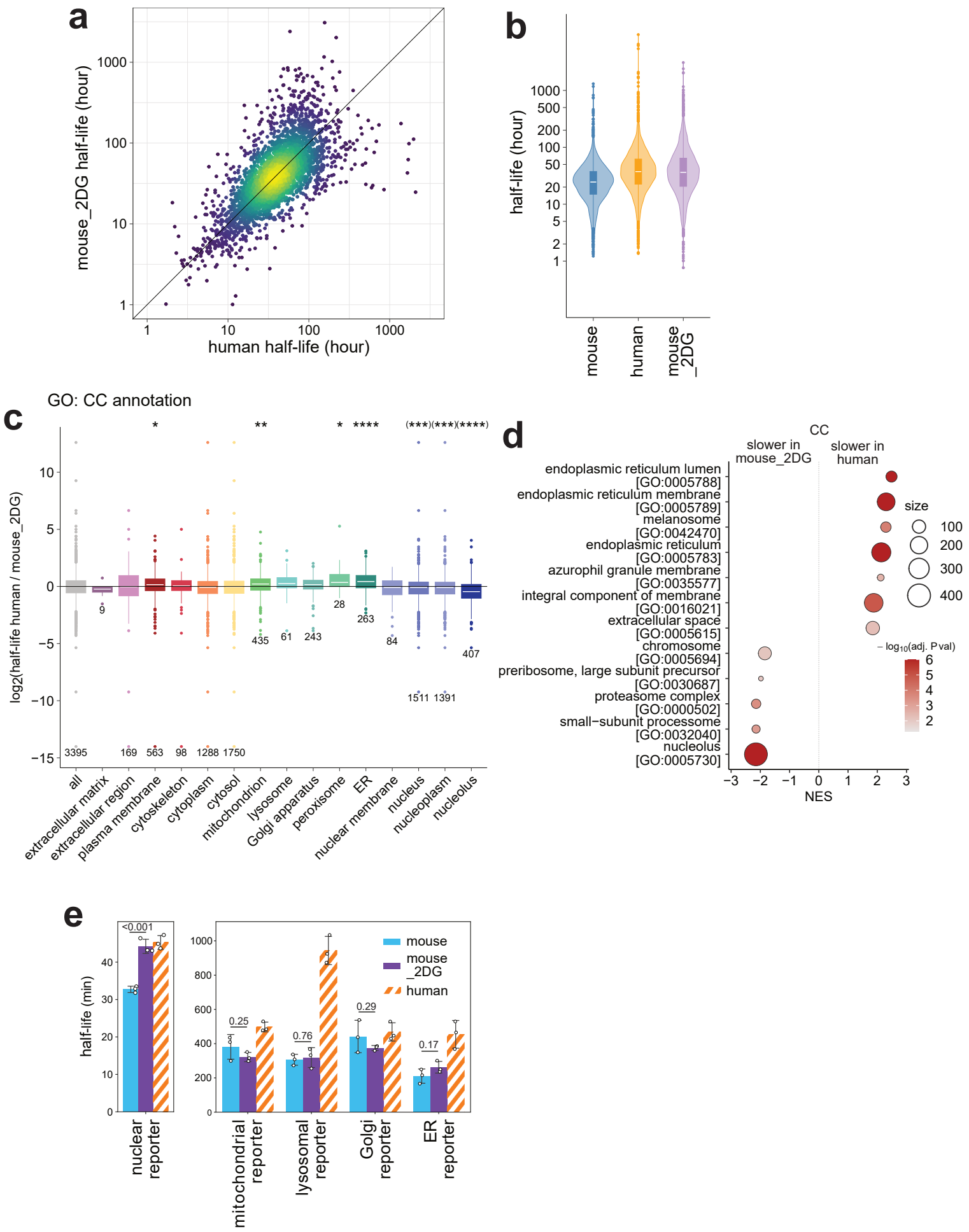
a
mouse_2DG half-life (hour)
human half-life (hour)
b
half-life (hour)
mouse
human
mouse_2DG
c
GO: CC annotation
log2(half-life human / mouse_2DG)
all
extracellular matrix
extracellular region
plasma membrane
cytoskeleton
cytoplasm
cytosol
mitochondrion
lysosome
Golgi apparatus
peroxisome
ER
nuclear membrane
nucleus
nucleoplasm
nucleolus
d
CC
slower in mouse_2DG
slower in human
endoplasmic reticulum lumen [GO:0005788]
endoplasmic reticulum membrane [GO:0005789]
melanosome [GO:0042470]
endoplasmic reticulum [GO:0005783]
azurophil granule membrane [GO:0035577]
integral component of membrane [GO:0016021]
extracellular space [GO:0005615]
chromosome [GO:0005694]
preribosome, large subunit precursor [GO:0030687]
proteasome complex [GO:0000502]
small−subunit processome [GO:0032040]
nucleolus [GO:0005730]
size
− log10(adj. Pval)
NES
e
half-life (min)
<0.001
mouse
mouse_2DG
human
0.25
0.76
0.29
0.17
nuclear reporter
mitochondrial reporter
lysosomal reporter
Golgi reporter
ER reporter

Fig. 4